

1

2



CERN-EP-2022-234

01 November 2022

3

4

Collins and Sivers transverse-spin asymmetries in inclusive muoproduction of ρ^0 mesons

5

The COMPASS Collaboration

6

Abstract

7

8

9

10

11

12

13

14

The production of vector mesons in deep inelastic scattering is an interesting yet scarcely explored channel to study the transverse spin structure of the nucleon and the related phenomena. The COMPASS collaboration has performed the first measurement of the Collins and Sivers asymmetries for inclusively produced ρ^0 mesons. The analysis is based on the data set collected in deep inelastic scattering in 2010 using a 160 GeV/c μ^+ beam impinging on a transversely polarized NH_3 target. The ρ^0 mesons are selected from oppositely charged hadron pairs, and the asymmetries are extracted as a function of the Bjorken- x variable, the transverse momentum of the pair and the fraction of the energy z carried by the pair. Indications for positive Collins and Sivers asymmetries are observed.

15

(to be submitted to Phys. Lett. B)

16 **1 Introduction**

17 In semi-inclusive deep inelastic scattering (SIDIS) $lN \rightarrow l' h X$, a high-energy lepton l scatters off a
 18 target nucleon N , and in the final state the scattered lepton l' is observed in coincidence with at least
 19 one hadron h produced in the current fragmentation region. This process presently is the main tool
 20 to study the complete 3-dimensional structure of the nucleon, i.e. the transverse spin and transverse
 21 momentum distributions of partons, and the possible correlations between their spin, their motion, and
 22 the spin of the nucleon. In the present quantum chromodynamics (QCD) framework, such information
 23 is encoded in the Transverse Momentum Dependent Parton Distribution Functions (TMD PDFs). In
 24 SIDIS, the above mentioned correlations induce azimuthal asymmetries in the angular distributions of
 25 the produced hadrons, which are interpreted in terms of convolutions of TMD PDFs and Transverse
 26 Momentum Dependent Fragmentation Functions (TMD FFs).

27 Among the accessible asymmetries, the transverse spin asymmetries (TSAs), which arise for a trans-
 28 versely polarized target nucleon, have been extensively studied in recent years. In particular, the Collins
 29 asymmetry arises from the convolution between the chiral-odd transversity PDF h_1^q [1] and the chiral-odd
 30 and T-odd Collins FF $H_{1q}^{\perp h}$ [2]. The transversity PDF, which is the difference between the number density
 31 of partons with transverse spin parallel and antiparallel to the transverse spin of the parent nucleon, is
 32 the least known among the three collinear PDFs needed for the complete characterization of the nucleon
 33 structure at leading order. The Collins TMD FF describes the correlation between the transverse spin of
 34 a fragmenting quark and the transverse momentum of the produced hadron, and probes the quark-spin
 35 dependence of the fragmentation process.

36 Another important TSA is the Sivers asymmetry, which is interpreted as the convolution of the Sivers
 37 function $f_{1T}^{\perp q}$ [3], the TMD PDF that describes the transverse momentum distribution of an unpolarized
 38 quark in a transversely polarized nucleon, and the spin-averaged FF D_{1q}^h that describes the fragmentation
 39 of an unpolarized quark into an unpolarized hadron.

40 Collins and Sivers asymmetries have been measured since 2005, in particular in SIDIS off protons,
 41 deuterons or neutrons for unidentified charged hadrons and for identified pions, kaons and protons by the
 42 HERMES [4], COMPASS [5–7] and JLab [8] experiments. Phenomenological analyses of the Collins
 43 asymmetries and the corresponding asymmetries measured in e^+e^- annihilation to hadrons [9–11] have
 44 led to the extraction of both the transversity PDF and the Collins FF [12–15]. Similarly, from the
 45 HERMES and COMPASS measurements of the Sivers asymmetry, the Sivers function was extracted by
 46 several authors [16–20].

47 Relevant information on nucleon structure and the fragmentation process can also be obtained from
 48 measurements of TSAs in inclusive production of vector mesons in DIS [21]. The Collins asymmetry for
 49 vector mesons couples the transversity PDF to the Collins FF $H_{1q}^{\perp VM}$, which describes the fragmentation of
 50 a transversely polarized quark into a vector meson. The investigation of this channel could shed new light
 51 on the still poorly known quark-spin dependence of the fragmentation process. Model predictions based
 52 on the recursive string+ 3P_0 model of polarized quark fragmentation suggest that the Collins asymmetry
 53 for ρ mesons has the opposite sign compared to that of positive pions. Depending on the choice of the
 54 parameters, the Collins asymmetry for vector meson production can be as large as for positive pions
 55 [22, 23].

56 Up to now, transverse spin asymmetries for vector meson production have not been measured, neither in
 57 SIDIS nor in e^+e^- annihilation into hadrons. The low statistics of the produced vector mesons and the
 58 high combinatorial background make the measurement of these asymmetries very challenging.

59 In this article we present the first measurement of the Collins and Sivers asymmetries for ρ^0 mesons
 60 produced in DIS off a transversely polarized proton target. The analysis is performed on the COMPASS
 61 data collected in 2010. The same data have already been used for many published results, e.g., the Collins

62 and Sivers asymmetries for unidentified charged hadrons [5, 6], pions and kaons [7], and dihadron
 63 production asymmetries [24]. The final data set used for the analysis described in this paper consists of
 64 2.6×10^6 ρ^0 mesons.

65 The article is organized as follows. The formalism of vector meson production in SIDIS is introduced
 66 in Sec. 2. Section 3 describes the experimental apparatus and the data set used for this analysis. The
 67 method used for the extraction of TSAs is explained in Sec. 4. The extraction of the ρ^0 signal is described
 68 in Sec. 5 and the results for Collins and Sivers ρ^0 asymmetries are given in Sec. 6. In Sec. 7 conclusions
 69 are drawn.

70 2 Theoretical formalism

71 The kinematics for the production of a vector meson (VM) in SIDIS off transversely polarised protons in
 72 the one-photon exchange approximation is schematically shown in Fig. 1. The process is represented in
 73 the gamma-nucleon system (GNS), namely in the reference system where the momentum of the exchanged
 74 virtual photon defines the \hat{z} axis and the \hat{x} - \hat{z} plane is the lepton scattering plane with the \hat{x} axis along
 75 the transverse component of the lepton momenta [25]. If the polarisation of the vector meson is not
 76 considered, the leading twist differential cross section has a similar expression to that of spinless hadrons
 77 [26]:

$$\begin{aligned} \frac{d^6\sigma}{dx dy dz dP_T^2 d\phi_{\text{VM}} d\phi_S} &= \frac{\alpha^2}{xyQ^2} \left(\frac{1+(1-y)^2}{2} \right) \times \left\{ \sum_q e_q^2 C \left[f_1^q D_{1q}^{\text{VM}} \right] \right. \\ &+ D_{\text{NN}} |\mathcal{S}_T| \sum_q e_q^2 C \left[\frac{\mathbf{p}_\perp \cdot \mathbf{P}_T}{z M_{\text{VM}} P_T} h_1^q H_{1q}^{\perp \text{VM}} \right] \sin(\phi_{\text{VM}} + \phi_S - \pi) \\ &\left. + |\mathcal{S}_T| \sum_q e_q^2 C \left[\frac{\mathbf{k}_T \cdot \mathbf{P}_T}{M P_T} f_{1T}^{\perp q} D_{1q}^{\text{VM}} \right] \sin(\phi_{\text{VM}} - \phi_S) + \dots \right\}. \quad (1) \end{aligned}$$

78 Here, x is the Bjorken variable, y is the fraction of the initial lepton energy loss in the target rest frame,
 79 and Q^2 is the virtuality of the photon. The variable z is the fraction of the energy of the virtual photon
 80 carried by the produced VM in the target rest frame and P_T is the modulus of its transverse momentum
 81 \mathbf{P}_T in the GNS. The variables ϕ_{VM} and ϕ_S are the azimuthal angle of \mathbf{P}_T and the one of the target
 82 transverse polarisation \mathcal{S}_T in the GNS, respectively. The combinations of angles $\phi_{\text{Coll}} = \phi_{\text{VM}} + \phi_S - \pi$
 83 and $\phi_{\text{Siv}} = \phi_{\text{VM}} - \phi_S$ are the Collins angle and the Sivers angle associated to the transverse momentum
 84 of the VM, respectively, and $D_{\text{NN}} = 2(1-y)/[1+(1-y)^2]$ is the virtual photon depolarisation factor.
 85 The nucleon mass and the mass of the vector meson are denoted as M and M_{VM} , respectively. The
 86 summations run over the quark and antiquark flavours and the (anti)quark charge e_q is given in units
 87 of the elementary charge. The cross section in Eq. (1) is written in terms of structure functions each

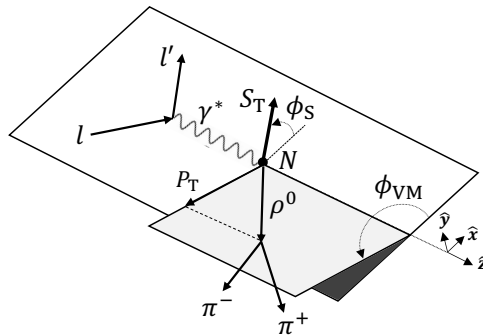


Fig. 1: Kinematics of the SIDIS process for ρ^0 meson production in the gamma-nucleon reference system.

88 involving the convolution

$$C [w f D] = \int d^2 \mathbf{k}_T d^2 \mathbf{p}_\perp \delta^{(2)}(z \mathbf{k}_T + \mathbf{p}_\perp - \mathbf{P}_T) w(\mathbf{k}_T, \mathbf{p}_\perp) x f(x, \mathbf{k}_T) D(z, \mathbf{p}_\perp), \quad (2)$$

89 where f indicates a TMD PDF, D indicates a TMD FF, and w is a weight factor depending on the intrinsic
90 quark transverse momentum \mathbf{k}_T in the GNS and on the transverse momentum \mathbf{p}_\perp of the VM with respect
91 to the direction of the scattered quark.

92 The expression for the Collins asymmetry can be obtained from the ratio between the transverse-spin-
93 dependent and the spin-averaged terms of the cross section in Eq. (1), and is given by

$$A_{\text{UT}}^{\sin \phi_{\text{Coll}}}(x, z, P_T) = \frac{\sum_q e_q^2 C \left[\frac{\mathbf{p}_\perp \cdot \mathbf{P}_T}{z M_{\text{VM}} P_T} h_1^q H_{1q}^{\perp \text{VM}} \right]}{\sum_q e_q^2 C \left[f_1^q D_{1q}^{\text{VM}} \right]}. \quad (3)$$

94 The functions D_{1q}^{VM} and $H_{1q}^{\perp \text{VM}}$ describe the fragmentation of an unpolarized and a transversely polarized
95 quark q into a vector meson, respectively.

96 The Sivers asymmetry reads [26]

$$A_{\text{UT}}^{\sin \phi_{\text{Siv}}}(x, z, P_T) = \frac{\sum_q e_q^2 C \left[\frac{\mathbf{k}_T \cdot \mathbf{P}_T}{M P_T} f_{1T}^{\perp q} D_{1q}^{\text{VM}} \right]}{\sum_q e_q^2 C \left[f_1^q D_{1q}^{\text{VM}} \right]}. \quad (4)$$

97 The expected number of vector mesons is

$$N_{\text{VM}}(x, z, P_T, \phi_{\text{Coll}}, \phi_{\text{Siv}}) \propto \left(1 + D_{\text{NN}} f P_t A_{\text{UT}}^{\sin \phi_{\text{Coll}}} \sin \phi_{\text{Coll}} + f P_t A_{\text{UT}}^{\sin \phi_{\text{Siv}}} \sin \phi_{\text{Siv}} \right). \quad (5)$$

98 Here, f is the dilution factor that takes into account the fraction of polarisable protons in the target, and
99 P_t is the average transverse polarisation of the polarisable protons in the target.

100 For the specific case of ρ^0 meson production considered in this work, we use all oppositely charged hadron
101 pairs in the event. The four-momentum of the ρ^0 candidate is given by $P_{h_1} + P_{h_2}$, where P_{h_1} and P_{h_2} are the
102 momenta of the positive and the negative hadron of the pair, respectively. The fractional energy of the ρ^0
103 candidate is given by $z = z_{h_1} + z_{h_2}$ and its transverse momentum in the GNS is given by $\mathbf{P}_T = \mathbf{P}_{h_1 T} + \mathbf{P}_{h_2 T}$,
104 where we have indicated by z_{h_i} and $\mathbf{P}_{h_i T}$ ($i = 1, 2$) the fraction of the virtual photon energy carried by the
105 hadron h_i in the target rest system, and the transverse momentum of h_i in the GNS, respectively. In the
106 following we indicate with ϕ_{hh} the azimuthal angle of \mathbf{P}_T , and with $M_{\text{hh}} = \sqrt{(P_{h_1} + P_{h_2})^2}$ the invariant
107 mass of the pair. As it will be discussed in Sec. 5, the data set of ρ^0 candidates contains a sizeable
108 combinatorial background due to non-resonant hadron pairs.

109 3 Experimental apparatus and data sample

110 The COMPASS experiment, a fixed target experiment located at the M2 beamline of the CERN SPS,
111 is in operation since 2002. A detailed description of the apparatus can be found in Ref. [5, 7, 27].
112 The data used in this analysis were collected in 2010 using a 160 GeV/c μ^+ beam and a transversely
113 polarized NH_3 target. The target consisted of three cylindrical cells with neighbouring cells polarized in
114 opposite directions in order to collect data simultaneously for both target spin orientations. The average
115 polarisation of the hydrogen nuclei was $\langle P_t \rangle \simeq 0.8$ and the average dilution factor was $\langle f \rangle \simeq 0.15$. The
116 data taking was divided in twelve periods of about ten days. In order to compensate for acceptance effects
117 the polarisation was reversed in the middle of each period.

118 Only events with an incoming and an outgoing muon track and at least two produced charged hadrons are
 119 considered. Equal flux along the target cells is assured by requiring the extrapolated incoming muon to
 120 cross all three target cells. Tracks from mesons produced in weak decays are rejected, as we only consider
 121 hadrons coming from the production vertex. In order to ensure the deep inelastic regime, we require
 122 $Q^2 > 1.0(\text{GeV}/c)^2$ and the invariant mass of the final hadronic system $W > 5 \text{ GeV}/c^2$. The Bjorken x
 123 variable ranges between 0.003 and 0.7. The selection $y > 0.1$ removes events with poorly reconstructed
 124 virtual photon energy and $y < 0.9$ removes events with large radiative effects. For hadrons, we require
 125 $z_h > 0.1$ to ensure the current fragmentation regime and $P_{hT} > 0.1 \text{ GeV}/c$ to ensure good resolution in
 126 the respective azimuthal angle.

127 The dihadron samples with pairs h^+h^- , h^+h^+ , h^-h^- of charged hadrons are selected as described in the
 128 following. In order to avoid the contribution from non-SIDIS diffractive events, exclusively produced
 129 h^+h^- pairs are rejected by requiring a missing energy $E_{\text{miss}} > 3.0 \text{ GeV}$, where $E_{\text{miss}} = (M_X^2 - M^2)/2M$,
 130 and $M_X^2 = (q + P_p - P)^2$ where q , P_p and P are the four momenta of the exchanged photon, the target
 131 proton and the hadron pair respectively. The requirements $z < 0.95$, $0.1 \text{ GeV}/c < P_T < 4.0 \text{ GeV}/c$ and
 132 $0.35 \text{ GeV}/c^2 < M_{\text{hh}} < 3.0 \text{ GeV}/c^2$ are also applied in order to define the kinematic range of the analysis.
 133 The selection $z > 0.3$ is applied in order to enhance the fraction of ρ^0 mesons. No further selection
 134 improving the signal over background ratio could be found.

135 The selected dihadron samples consist of about 3.4×10^7 h^+h^- pairs, 1.1×10^7 h^+h^+ pairs and 0.7×10^7
 136 h^-h^- pairs. The distributions of x , z and P_T for the selected h^+h^- sample are shown as filled histograms
 137 in the left, middle and right panels of Fig. 2, respectively. The empty histogram in the middle panel
 138 of the same figure shows the z distribution without the requirements on the hadron pairs. The exclusive
 139 peak at $z = 1$, rejected by the requirement on the missing energy, is clearly visible.

140 The invariant mass distribution for the h^+h^- sample is shown in Fig. 3, where the empty (filled) histogram
 141 is the invariant mass distribution before (after) the application of the cuts on the hadron pair variables.
 142 The peak corresponding to the $\rho^0(770)$ invariant mass is clearly visible as well as the broad structures
 143 corresponding to the $f_0(980)$ and $f_2(1240)$ mesons. As the requirement of the missing energy rejects
 144 exclusive events, it also reduces the significance of the ρ^0 peak.

145 4 Method for the extraction of the transverse spin asymmetries

146 The invariant mass range is divided in the four regions that are defined in Tab. 1 and shown in Fig. 3 as
 147 separated by the vertical lines. Region II covers the ρ^0 invariant mass peak and will be referred to as the
 148 “ ρ^0 region” in the following. Regions I and III are dominated by the combinatorial background and in
 149 the following will be referred to as the “side band” regions. Region IV has the same statistics as region

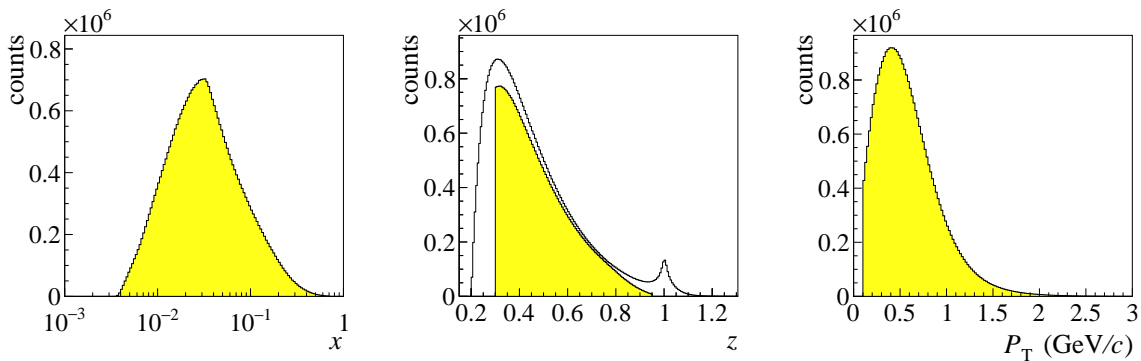


Fig. 2: Distributions of x (left panel), z (middle panel) and P_T (right panel) for the selected h^+h^- pairs (filled histograms). The empty histogram in the middle panel shows the z distribution before applying the requirements on hadron pairs.

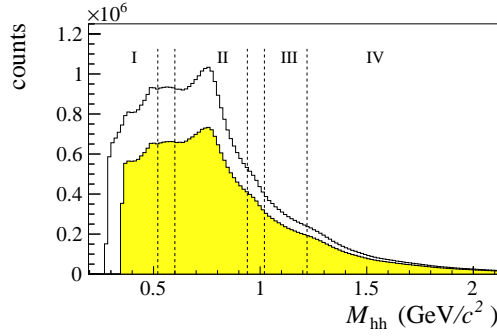


Fig. 3: Invariant mass distribution of h^+h^- pairs before (empty histogram) and after (filled histogram) applying the requirements on the hadron pair variables. The vertical lines indicate the different invariant mass regions defined in Tab. 1.

150 III and is included to study the invariant mass dependence of TSAs for the combinatorial background,
 151 although it is not used in the extraction of the ρ^0 asymmetries.

152 The extraction of the ρ^0 TSAs proceeds using the following steps. First, the fraction f_s of ρ^0 mesons
 153 in the ρ^0 region is evaluated. Then, the transverse spin asymmetry $a_{\text{UT}}^{\sin\phi_X}$ of the h^+h^- pairs in the ρ^0
 154 region is extracted. The angle ϕ_X indicates either the Collins angle ϕ_{Coll} or the Sivers angle ϕ_{Siv} . The
 155 asymmetries are measured for all kinematic bins by using the unbinned maximum likelihood method
 156 [28] and the fit function $F(\phi_{\text{Coll}}, \phi_{\text{Siv}}) = a_0 \times (1 + a_C \sin\phi_{\text{Coll}} + a_S \sin\phi_{\text{Siv}})$ in agreement with the r.h.s.
 157 of Eq. (5). The parameters a_0 , a_C and a_S are determined from the fitting procedure and are used to
 158 calculate the asymmetries $a_{\text{UT}}^{\sin\phi_{\text{Coll}}} = a_C / (\langle f \rangle \langle D_{\text{NN}} \rangle \langle P_t \rangle)$ and $a_{\text{UT}}^{\sin\phi_{\text{Siv}}} = a_S / (\langle f \rangle \langle P_t \rangle)$. The transverse
 159 spin asymmetry $A_{\text{UT,bg}}^{\sin\phi_X}$ of the background is evaluated as the mean of the asymmetries in regions I and
 160 III using the same procedure. In order to obtain the asymmetry for ρ^0 mesons, the background transverse
 161 spin asymmetry is subtracted from the asymmetry in the ρ^0 region according to

$$A_{\text{UT}}^{\sin\phi_X} = \left[a_{\text{UT}}^{\sin\phi_X} - (1 - f_s) A_{\text{UT,bg}}^{\sin\phi_X} \right] \times \frac{1}{f_s}. \quad (6)$$

Region	Invariant mass range
I	$0.35 \text{ GeV}/c^2 < M_{\text{hh}} < 0.52 \text{ GeV}/c^2$
II	$0.60 \text{ GeV}/c^2 < M_{\text{hh}} < 0.94 \text{ GeV}/c^2$
III	$1.02 \text{ GeV}/c^2 < M_{\text{hh}} < 1.22 \text{ GeV}/c^2$
IV	$1.22 \text{ GeV}/c^2 < M_{\text{hh}} < 3.00 \text{ GeV}/c^2$

Table 1: Invariant mass regions used in the extraction of the asymmetries.

162 5 Estimation of the ρ^0 signal

163 In order to determine the fraction of ρ^0 mesons in the invariant mass region II, it is necessary to evaluate the
 164 contribution of the combinatorial background. The shape of the background distribution in the ρ^0 region
 165 is taken from the sum of the invariant mass distributions of h^+h^+ and h^-h^- pairs. As normalisation the
 166 ratio between the number of h^+h^- pairs and the number of like-sign pairs in the invariant mass interval
 167 $0.5 \text{ GeV}/c^2 < M_{\text{hh}} < 0.58 \text{ GeV}/c^2$ is used, where the ratio between the invariant mass distributions of
 168 opposite and like-sign pairs is constant. For $M_{\text{hh}} < 0.50 \text{ GeV}/c^2$ the background subtraction procedure
 169 yields negative counts, meaning that the estimated background is larger than the h^+h^- distribution. The
 170 distribution of like-sign pairs is in fact not expected to reproduce the full invariant mass spectrum, but

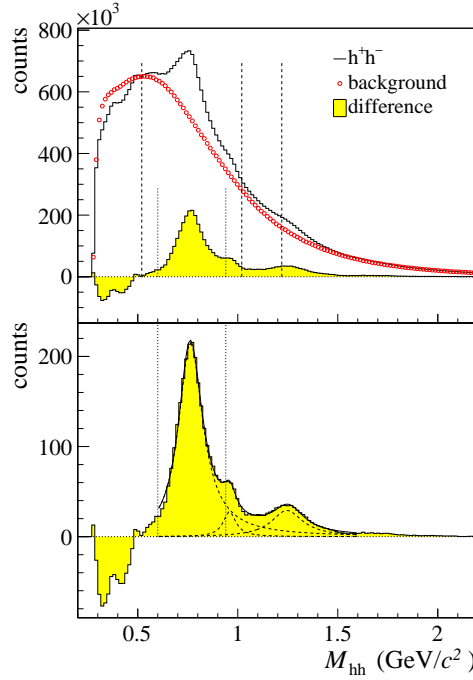


Fig. 4: Top panel: the invariant mass distribution of h^+h^- pairs (empty histogram), the background distribution (red points) and the difference between the two distributions (filled histogram). Bottom panel: zoom of the difference distributions. The vertical lines show the invariant mass regions defined in Tab. 1. See text for more details.

171 only that below the ρ^0 peak. The estimated invariant mass distribution of the background is shown in the
 172 top panel of Fig. 4 by the red points. It is subtracted from the h^+h^- distribution (continuous histogram) to
 173 obtain the difference of the distributions shown by the filled histogram. After checking the compatibility
 174 of the invariant mass distributions in the different data taking periods, this procedure is performed on the
 175 invariant mass distributions integrated over the full year of data taking.

176 In the difference of distributions, shown more clearly in the bottom panel of Fig. 4, the peak corresponding
 177 to the $\rho^0(770)$ meson is clearly visible. Also visible are the structures corresponding to the $f_0(980)$ and
 178 $f_2(1270)$ mesons. The difference of the distributions is fitted successfully by a sum of three Breit-
 179 Wigner functions¹, demonstrating that the subtraction procedure is clean. In each Breit-Wigner function
 180 the parameters corresponding to the nominal mass and the width of the resonance are fixed to the
 181 corresponding PDG values, and only the normalisation parameter is estimated by the fit procedure. The
 182 fit function is shown by the continuous line, and the separate contributions of the ρ^0 , f_0 and f_2 mesons
 183 are shown by the dashed lines. The fact that the extracted ρ^0 distribution can be successfully described by
 184 a Breit-Wigner function provides confirmation that the form of the combinatorial background in region
 185 II and its normalisation is evaluated correctly.

186 The fraction f_s of ρ^0 mesons in region II is calculated by dividing the number of ρ^0 mesons by the total
 187 number of h^+h^- pairs in the same region. The contamination from the decay of f_0 mesons, estimated to
 188 be about 4%, is neglected. Also, since the ρ^0 distribution is described by a width fixed to the PDG value,
 189 possible interference effects with the $\omega(782)$ decays are neglected. The total number of ρ^0 mesons is
 190 estimated to be 2.6×10^6 and the average signal fraction is $\langle f_s \rangle = 0.18$.

¹A p -wave Breit-Wigner function is used to describe the ρ^0 peak and a s -wave Breit-Wigner function is employed to describe the f_0 and f_2 peaks.

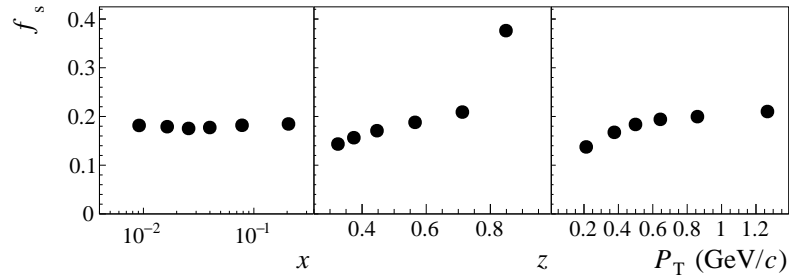


Fig. 5: The ρ^0 signal fraction as a function of x (left), z (middle) and P_T (right).

191 This procedure is applied to all x , z and P_T bins, and the values of f_s are shown in Fig. 5. We find f_s
 192 to be almost constant and about 0.18 as a function of x and it increases with P_T and z . The high value
 193 (about 0.38) in the last z bin can be understood in terms of the string fragmentation model, where heavier
 194 resonances are produced mostly with large fractional energies [29].

195 As consistency check we compared the counts of ρ^0 mesons obtained by summing separately over the x ,
 196 z and P_T bins, which results in similar values that differ by less than 2% with respect to the integrated
 197 value. As a further check, the measured ρ^0 distribution is compared for each kinematic bin to that
 198 expected by using a Breit-Wigner function with mass peak and width fixed to the PDG values and the
 199 normalisation fitted to the measured ρ^0 distribution in the ρ^0 region. The largest differences on the
 200 ρ^0 counts are found to be less than 7.5% and located in the first two z bins. These differences are
 201 taken into account in the evaluation of the systematic uncertainty of the final asymmetries. Moreover,
 202 it is checked that nearly the same background in the ρ^0 region can be obtained with an alternative
 203 method that combines the invariant mass distributions simulated with the PYTHIA 8 event generator [30]
 204 for the different background components (resonant and non-resonant contributions) and Breit-Wigner
 205 functions with PDG parameters for the ρ^0 , f_0 and f_2 resonances to fit the total h^+h^- distribution up to
 206 $M_{hh} = 1.4 \text{ GeV}/c^2$. The differences between the two methods are small and are taken into account in the
 207 systematic uncertainty of the measured asymmetries for ρ^0 mesons.

208 6 Results for Collins and Sivers asymmetries

209 The Collins asymmetry $a_{\text{UT}}^{\sin\phi_{\text{Coll}}}$ for all selected h^+h^- pairs is shown in Fig. 6 as a function of x , z , P_T
 210 and M_{hh} . The asymmetries are evaluated in each of the twelve periods of data taking and the final result
 211 is obtained as the weighted average. Each row corresponds to a different invariant mass region. Starting
 212 from the top, the second row shows the asymmetry in the ρ^0 region, which has mostly positive values,
 213 in particular around $z \sim 0.3$ and for $P_T < 0.5 \text{ GeV}/c$. This is at variance with the asymmetries in the
 214 side band regions, shown in the first and third rows, which tend to be negative. Also, these asymmetries
 215 in the side band regions are similar. No strong kinematic dependence with the invariant mass is found.
 216 This is demonstrated by the invariant-mass dependence in the rightmost column. No significant effect is
 217 observed at large invariant mass, as can be seen from the bottom row.

218 The background asymmetry is evaluated taking the average of the asymmetries in regions I and III.
 219 According to Eq. (6), the background asymmetry is first rescaled by the factor $1 - f_s$ and then subtracted
 220 from the Collins asymmetry in the ρ^0 region. The contribution of the background asymmetry in the
 221 ρ^0 region is shown in the top panel of Fig. 7 as a function of x , z and P_T . It has mostly negative
 222 values, as expected from Fig. 6, although the uncertainties are large. The final Collins asymmetry for
 223 ρ^0 mesons is shown in the bottom panel of Fig. 7 and the corresponding values are given in Tab. 2.
 224 Given the large uncertainties, no clear trend can be seen as a function of x and z . As a function of

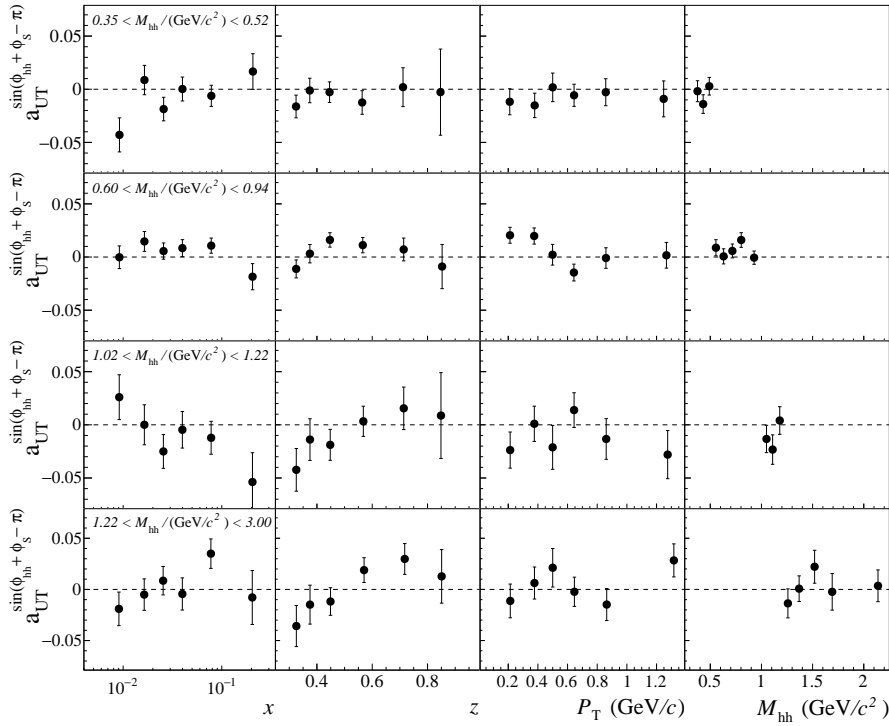


Fig. 6: Collins asymmetry for h^+h^- pairs as a function of the kinematic variables x , z , P_T and the invariant mass M_{hh} (columns from left to right). The different rows correspond to the invariant mass regions defined in Sec. 4. Only the statistical uncertainties are shown.

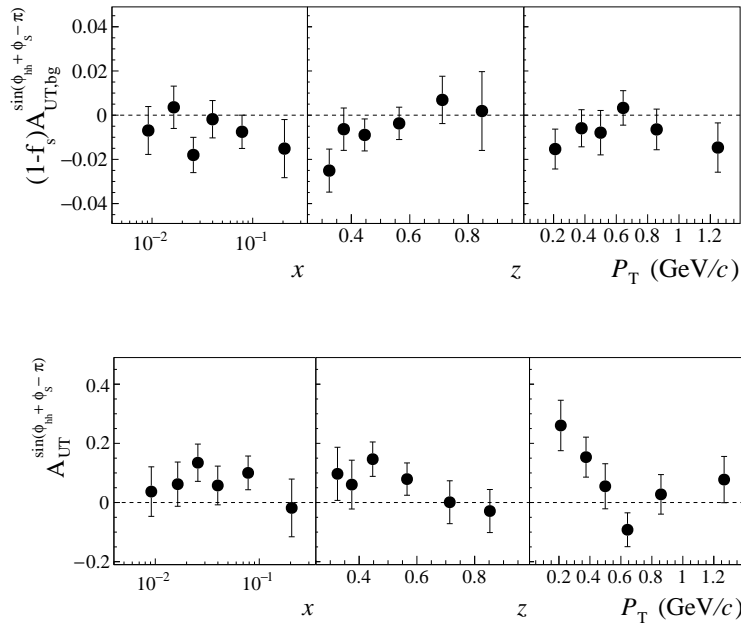


Fig. 7: The background contribution to the Collins asymmetry in the ρ^0 region (top panel) and the final Collins asymmetry for ρ^0 mesons (bottom panel) as a function of x , z and P_T . Only the statistical uncertainties are shown. The systematic uncertainty on the Collins asymmetry for ρ^0 mesons is estimated to be about 0.6 the statistical one.

x -bin	$\langle x \rangle$	$\langle z \rangle$	$\langle P_T \rangle / (\frac{\text{GeV}}{c})$	$\langle Q^2 \rangle / (\frac{\text{GeV}}{c})^2$	$A_{\text{UT}}^{\sin \phi_{\text{Coll}}}$	$A_{\text{UT}}^{\sin \phi_{\text{Siv}}}$
[0.003, 0.013)	0.009	0.47	0.60	1.44	0.037 ± 0.084	0.050 ± 0.062
[0.013, 0.020)	0.016	0.48	0.58	1.81	0.062 ± 0.075	0.072 ± 0.066
[0.020, 0.032)	0.026	0.48	0.56	2.16	0.134 ± 0.063	0.076 ± 0.058
[0.032, 0.050)	0.040	0.48	0.54	2.89	0.058 ± 0.065	0.051 ± 0.062
[0.050, 0.130)	0.078	0.48	0.54	5.49	0.100 ± 0.057	0.056 ± 0.054
[0.130, 0.700]	0.205	0.48	0.56	14.84	-0.018 ± 0.097	-0.030 ± 0.092
z -bin	$\langle x \rangle$	$\langle z \rangle$	$\langle P_T \rangle / (\frac{\text{GeV}}{c})$	$\langle Q^2 \rangle / (\frac{\text{GeV}}{c})^2$	$A_{\text{UT}}^{\sin \phi_{\text{Coll}}}$	$A_{\text{UT}}^{\sin \phi_{\text{Siv}}}$
[0.30, 0.35)	0.046	0.32	0.53	3.84	0.097 ± 0.090	0.031 ± 0.079
[0.35, 0.40)	0.048	0.37	0.54	3.85	0.061 ± 0.082	0.096 ± 0.073
[0.40, 0.50)	0.050	0.45	0.56	3.86	0.146 ± 0.058	0.104 ± 0.052
[0.50, 0.65)	0.052	0.57	0.58	3.83	0.079 ± 0.054	0.037 ± 0.049
[0.65, 0.80)	0.052	0.71	0.59	3.70	0.001 ± 0.072	-0.055 ± 0.066
[0.80, 0.95]	0.038	0.85	0.54	3.33	-0.029 ± 0.073	0.025 ± 0.065
P_T -bin ($\frac{\text{GeV}}{c}$)	$\langle x \rangle$	$\langle z \rangle$	$\langle P_T \rangle / (\frac{\text{GeV}}{c})$	$\langle Q^2 \rangle / (\frac{\text{GeV}}{c})^2$	$A_{\text{UT}}^{\sin \phi_{\text{Coll}}}$	$A_{\text{UT}}^{\sin \phi_{\text{Siv}}}$
[0.10, 0.30)	0.050	0.47	0.21	3.58	0.260 ± 0.085	0.109 ± 0.078
[0.30, 0.45)	0.050	0.48	0.37	3.65	0.153 ± 0.068	0.075 ± 0.061
[0.45, 0.55)	0.050	0.48	0.50	3.73	0.055 ± 0.076	0.056 ± 0.069
[0.55, 0.75)	0.050	0.48	0.64	3.84	-0.092 ± 0.057	0.034 ± 0.051
[0.75, 1.00)	0.049	0.49	0.86	4.04	0.028 ± 0.067	0.065 ± 0.059
[1.00, 4.00]	0.047	0.50	1.27	4.49	0.077 ± 0.078	-0.048 ± 0.067

Table 2: The measured values of the Collins and Sivers asymmetries for ρ^0 mesons as a function of x , z and P_T . Shown are also the definitions of the x , z and P_T bins, as well as the average values $\langle x \rangle$, $\langle z \rangle$, $\langle P_T \rangle$ and $\langle Q^2 \rangle$ for each kinematic bin. Only the statistical uncertainties of the asymmetries are given. The systematic uncertainty is estimated to be about 0.6 the statistical one.

225 P_T the asymmetry increases for $P_T < 0.5 \text{ GeV}/c$, as suggested by the simulations carried out with the
 226 recursive string+ 3P_0 model in Ref. [23], using the scenario where the production of vector mesons with
 227 longitudinal polarization in the GNS is favoured.

228 The systematic uncertainty on the extracted transverse spin asymmetries for ρ^0 mesons is estimated to
 229 be about 0.6 times the statistical one. As described above, this estimate accounts for the systematic
 230 uncertainty on the evaluation of the background distribution in the ρ^0 region. In addition it takes into
 231 account other sources of systematic uncertainties, such as the period by period compatibility of the
 232 asymmetries and variations on the ρ^0 asymmetries induced by changing the invariant mass interval
 233 corresponding to the region II.

234 The average value of the Collins asymmetry for ρ^0 mesons is shown in Fig. 8. The asymmetry is positive
 235 with a significance of 2.3 standard deviations, evaluated taking into account both statistical and systematic
 236 uncertainties, and is in agreement with the model predictions [22]. Comparing the average value of the
 237 measured ρ^0 Collins asymmetry with that of the simulated one [23], shown as the open point in Fig. 8,
 238 consistency is found within about one standard deviation.

239 The same procedure is repeated for the Sivers asymmetry. The asymmetry $a_{\text{UT}}^{\sin \phi_{\text{Siv}}}$ is shown as a function
 240 of x , z , P_T and M_{hh} in Fig. 9 for the different invariant mass regions. The Sivers asymmetry in the ρ^0
 241 region exhibits positive values and a clear trend with x . Contrary to the case of the Collins asymmetry, the
 242 Sivers asymmetry is positive and significant also in the side-bands. This indicates that the contribution
 243 of the background to the asymmetry is large in the ρ^0 region, as shown in the top panel of Fig. 10. The
 244 background-subtracted final Sivers asymmetry for ρ^0 mesons is shown in the bottom panel in Fig. 10
 245 and the corresponding values are given in Tab. 2. The shown uncertainties are the statistical ones. As

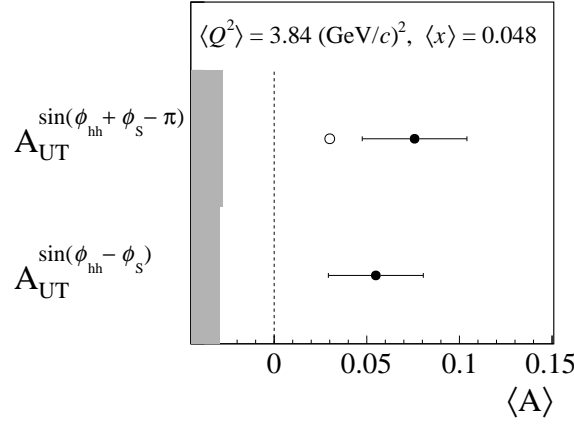


Fig. 8: Average values of the Collins and Sivers asymmetries for ρ^0 mesons. The gray bands represent the evaluated systematic uncertainty. The open point shows the average Collins asymmetry from simulations.

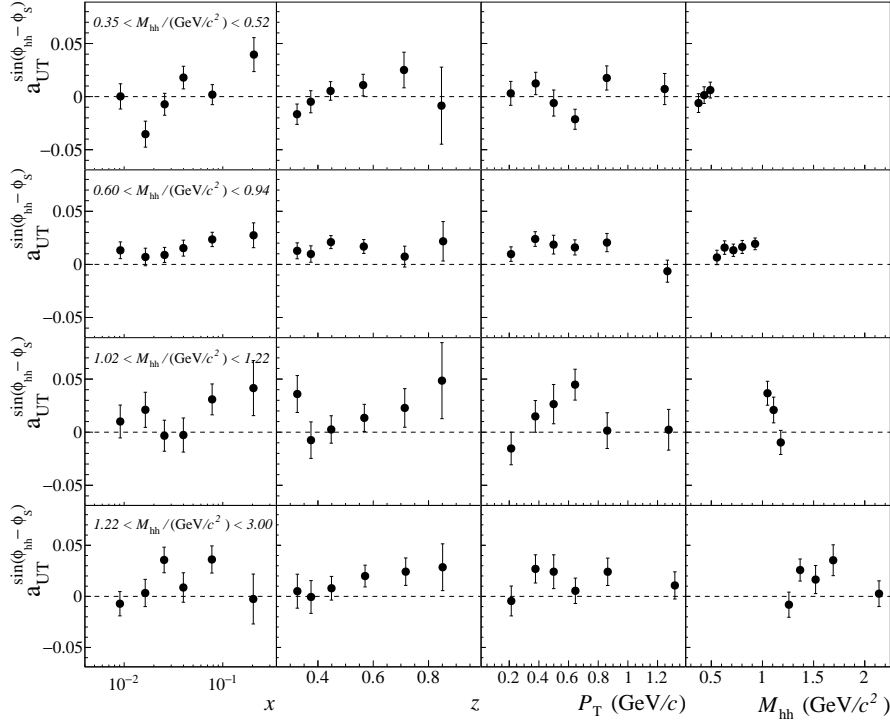


Fig. 9: Sivers asymmetry for h^+h^- pairs as a function of the kinematic variables x , z , P_T and the invariant mass M_{hh} (columns from left to right). The different rows correspond to the invariant mass regions defined in Sec. 4. Only the statistical uncertainties are shown.

246 for the Collins asymmetry, the systematic uncertainty is evaluated to be 0.6 times the statistical one. The
 247 average value of the asymmetry is shown in Fig. 8. It is found to be positive with a significance of 1.8
 248 standard deviations. A positive Sivers asymmetry for ρ^0 mesons is expected because, by momentum
 249 conservation in the hard scattering, the Sivers function induces a modulation on the direction of the struck
 250 quark which propagates to all the hadrons produced in the fragmentation process. The Sivers asymmetry
 251 for ρ^0 mesons is thus naively expected to be similar to the average value of the Sivers asymmetries for
 252 positive and negative pions, which is positive [7]. Given the large uncertainties, no clear trends as a
 253 function of the kinematic variables can be seen for the ρ^0 asymmetry.

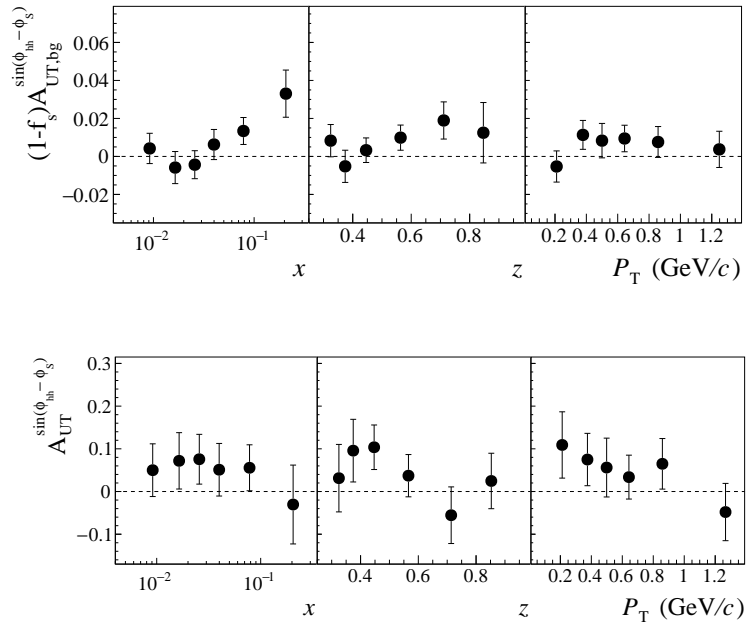


Fig. 10: The background contribution to the Sivers asymmetry in the ρ^0 region (top panel) and the final Sivers asymmetry for ρ^0 mesons (bottom panel) as a function of x , z and P_T . Only the statistical uncertainties are shown. The systematic uncertainty on the Sivers asymmetry for ρ^0 mesons is estimated to be about 0.6 the statistical one.

254 7 Conclusions

255 The COMPASS Collaboration has performed the first measurement of the Collins and Sivers transverse
 256 spin asymmetries for ρ^0 mesons produced in DIS off transversely polarized protons. The full data set
 257 of SIDIS events collected by COMPASS in 2010 was analysed. An indication for a positive Collins
 258 asymmetry is found. The result is in agreement with the expectation from the recursive string+ 3P_0 model
 259 of the polarized quark fragmentation process. Also an indication for a positive Sivers asymmetry is
 260 found, in agreement with the parton model. This work shows that the measurement of TSAs for inclusive
 261 vector meson production in DIS is feasible and could be done with higher precision at future facilities.

262 Acknowledgements

263 This work was made possible thanks to the financial support of our funding agencies. We also acknowledge
 264 the support of the CERN management and staff, as well as the skills and efforts of the technicians of the
 265 collaborating institutes.

266 References

- 267 [1] R. L. Jaffe, X.-D. Ji, Chiral odd parton distributions and polarized Drell-Yan, Phys. Rev. Lett. 67
 268 (1991) 552–555. doi:[10.1103/PhysRevLett.67.552](https://doi.org/10.1103/PhysRevLett.67.552).
- 269 [2] J. C. Collins, Fragmentation of transversely polarized quarks probed in transverse momentum
 270 distributions, Nucl. Phys. B396 (1993) 161–182. doi:[10.1016/0550-3213\(93\)90262-N](https://doi.org/10.1016/0550-3213(93)90262-N).
- 271 [3] D. W. Sivers, Single Spin Production Asymmetries from the Hard Scattering of Point-Like Con-
 272 stituents, Phys. Rev. D41 (1990) 83. doi:[10.1103/PhysRevD.41.83](https://doi.org/10.1103/PhysRevD.41.83).

- 273 [4] A. Airapetian, et al., Azimuthal single- and double-spin asymmetries in semi-inclusive deep-
274 inelastic lepton scattering by transversely polarized protons, JHEP 12 (2020) 010. doi:10.1007/
275 JHEP12(2020)010.
- 276 [5] C. Adolph, et al., Experimental investigation of transverse spin asymmetries in muon-p SIDIS
277 processes: Collins asymmetries, Phys. Lett. B 717 (2012) 376–382. doi:10.1016/j.physletb.
278 2012.09.055.
- 279 [6] C. Adolph, et al., II – Experimental investigation of transverse spin asymmetries in μ -p SIDIS
280 processes: Sivers asymmetries, Phys. Lett. B 717 (2012) 383–389. doi:10.1016/j.physletb.
281 2012.09.056.
- 282 [7] C. Adolph *et al.*, Collins and Sivers asymmetries in muonproduction of pions and kaons off trans-
283 versely polarised protons, *Phys. Lett.* B744 (2015) 250–259. doi:10.1016/j.physletb.2015.
284 03.056.
- 285 [8] X. Qian *et al.*, Single Spin Asymmetries in Charged Pion Production from Semi-Inclusive Deep
286 Inelastic Scattering on a Transversely Polarized ^3He Target, Phys. Rev. Lett. 107 (2011) 072003.
287 doi:10.1103/PhysRevLett.107.072003.
- 288 [9] A. Vossen, et al., Observation of transverse polarization asymmetries of charged pion pairs in
289 e^+e^- annihilation near $\sqrt{s} = 10.58$ GeV, Phys. Rev. Lett. 107 (2011) 072004. doi:10.1103/
290 PhysRevLett.107.072004.
- 291 [10] M. Ablikim, et al., Measurement of azimuthal asymmetries in inclusive charged dipion production
292 in e^+e^- annihilations at $\sqrt{s} = 3.65$ GeV, Phys. Rev. Lett. 116 (4) (2016) 042001. doi:10.1103/
293 PhysRevLett.116.042001.
- 294 [11] J. P. Lees, et al., Measurement of Collins asymmetries in inclusive production of charged pion pairs
295 in e^+e^- annihilation at BABAR, Phys. Rev. D90 (5) (2014) 052003. doi:10.1103/PhysRevD.
296 90.052003.
- 297 [12] M. Anselmino, M. Boglione, U. D’Alesio, J. O. Gonzalez Hernandez, S. Melis, F. Murgia,
298 A. Prokudin, Collins functions for pions from SIDIS and new e^+e^- data: a first glance at their trans-
299 verse momentum dependence, Phys. Rev. D 92 (11) (2015) 114023. doi:10.1103/PhysRevD.
300 92.114023.
- 301 [13] A. Martin, F. Bradamante, V. Barone, Extracting the transversity distributions from single-hadron
302 and dihadron production, Phys. Rev. D91 (1) (2015) 014034. doi:10.1103/PhysRevD.91.
303 014034.
- 304 [14] Z.-B. Kang, A. Prokudin, P. Sun, F. Yuan, Extraction of Quark Transversity Distribution and
305 Collins Fragmentation Functions with QCD Evolution, Phys. Rev. D 93 (1) (2016) 014009. doi:
306 10.1103/PhysRevD.93.014009.
- 307 [15] J. Cammarota, L. Gamberg, Z.-B. Kang, J. A. Miller, D. Pitonyak, A. Prokudin, T. C. Rogers, N. Sato,
308 Origin of single transverse-spin asymmetries in high-energy collisions, Phys. Rev. D 102 (5) (2020)
309 054002. doi:10.1103/PhysRevD.102.054002.
- 310 [16] M. Anselmino, M. Boglione, S. Melis, A Strategy towards the extraction of the Sivers function with
311 TMD evolution, Phys. Rev. D 86 (2012) 014028. doi:10.1103/PhysRevD.86.014028.
- 312 [17] P. Sun, F. Yuan, Energy Evolution for the Sivers Asymmetries in Hard Processes, Phys. Rev. D 88
313 (2013) 034016. doi:10.1103/PhysRevD.88.034016.

- 314 [18] M. G. Echevarria, A. Idilbi, Z.-B. Kang, I. Vitev, QCD Evolution of the Sivers Asymmetry, Phys.
315 Rev. D 89 (2014) 074013. doi:[10.1103/PhysRevD.89.074013](https://doi.org/10.1103/PhysRevD.89.074013).
- 316 [19] A. Martin, F. Bradamante, V. Barone, Direct extraction of the Sivers distributions from spin
317 asymmetries in pion and kaon leptonproduction, Phys. Rev. D 95 (9) (2017) 094024. doi:
318 [10.1103/PhysRevD.95.094024](https://doi.org/10.1103/PhysRevD.95.094024).
- 319 [20] M. G. Alexeev, et al., Measurement of P_T -weighted Sivers asymmetries in leptonproduction of
320 hadrons, Nucl. Phys. B 940 (2019) 34–53. doi:[10.1016/j.nuclphysb.2018.12.024](https://doi.org/10.1016/j.nuclphysb.2018.12.024).
- 321 [21] A. Bacchetta, P. J. Mulders, Deep inelastic leptonproduction of spin-one hadrons, Phys. Rev. D 62
322 (2000) 114004. doi:[10.1103/PhysRevD.62.114004](https://doi.org/10.1103/PhysRevD.62.114004).
- 323 [22] J. Czyzewski, Single spin asymmetry of vector meson production in the string model, Acta Phys.
324 Polon. 27 (1996) 1759–1766. arXiv:[hep-ph/9606390](https://arxiv.org/abs/hep-ph/9606390).
- 325 [23] A. Kerbizi, X. Artru, A. Martin, Production of vector mesons in the string+ 3P_0 model of polarized
326 quark fragmentation, Phys. Rev. D 104 (11) (2021) 114038. doi:[10.1103/PhysRevD.104.](https://doi.org/10.1103/PhysRevD.104.114038)
327 [114038](https://doi.org/10.1103/PhysRevD.104.114038).
- 328 [24] C. Adolph *et al.*, A high-statistics measurement of transverse spin effects in dihadron production
329 from muon–proton semi-inclusive deep-inelastic scattering, Phys. Lett. B736 (2014) 124–131.
330 doi:[10.1016/j.physletb.2014.06.080](https://doi.org/10.1016/j.physletb.2014.06.080).
- 331 [25] A. Bacchetta, U. D’Alesio, M. Diehl, C. A. Miller, Single-spin asymmetries: The Trento conventions,
332 Phys. Rev. D 70 (2004) 117504. doi:[10.1103/PhysRevD.70.117504](https://doi.org/10.1103/PhysRevD.70.117504).
- 333 [26] A. Bacchetta, M. Diehl, K. Goeke, A. Metz, P. J. Mulders, M. Schlegel, Semi-inclusive deep inelastic
334 scattering at small transverse momentum, JHEP 02 (2007) 093. doi:[10.1088/1126-6708/2007/](https://doi.org/10.1088/1126-6708/2007/02/093)
335 [02/093](https://doi.org/10.1088/1126-6708/2007/02/093).
- 336 [27] P. Abbon, et al., The COMPASS experiment at CERN, Nucl. Instrum. Meth. A 577 (2007) 455–518.
337 doi:[10.1016/j.nima.2007.03.026](https://doi.org/10.1016/j.nima.2007.03.026).
- 338 [28] M. Alekseev, et al., Collins and Sivers asymmetries for pions and kaons in muon-deuteron DIS,
339 Phys. Lett. B 673 (2009) 127–135. doi:[10.1016/j.physletb.2009.01.060](https://doi.org/10.1016/j.physletb.2009.01.060).
- 340 [29] B. Andersson, G. Gustafson, G. Ingelman, T. Sjostrand, Parton Fragmentation and String Dynamics,
341 Phys. Rept. 97 (1983) 31–145. doi:[10.1016/0370-1573\(83\)90080-7](https://doi.org/10.1016/0370-1573(83)90080-7).
- 342 [30] T. Sjostrand, S. Mrenna, P. Z. Skands, A Brief Introduction to PYTHIA 8.1, JHEP05 (2006) 026,
343 Comput. Phys. Commun. 178 (2008) 852–867. doi:[10.1016/j.cpc.2008.01.036](https://doi.org/10.1016/j.cpc.2008.01.036).